

# In Vivo Evaluation of a Gallium-68-Labeled Tumor-Tracking Cyanine Dye for Positron Emission Tomography/Near-Infrared Fluorescence Carcinoma Imaging, Image-Guided Surgery, and Photothermal Therapy

Jiaxu Zhu,<sup>§</sup> Yaqun Jiang,<sup>§</sup> Xin Pan, Kui Xu, Wenhao Niu, Yibing Lv, Chongjiao Li, Yichun Wang, Zejian Xue, Ping Lei,<sup>\*</sup> and Yong He<sup>\*</sup>



Cite This: *ACS Omega* 2023, 8, 6067–6077



Read Online

ACCESS |



Metrics & More

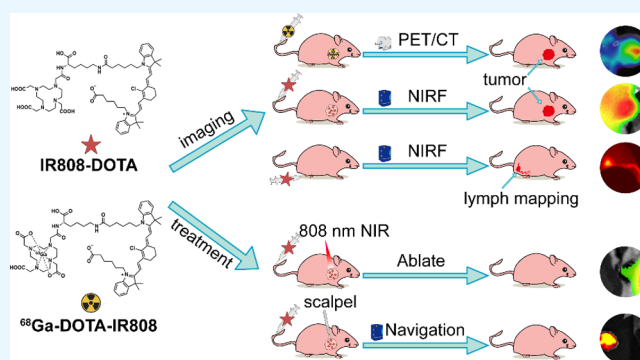


Article Recommendations



Supporting Information

**ABSTRACT:** Positron emission tomography (PET)/near-infrared fluorescence (NIRF) dual-modal imaging presents an enticing prospect for tumor diagnosis and surgical navigation. In this study, we developed a novel probe IR808-DOTA for tumor-targeted PET/NIRF imaging, image-guided surgery, and photothermal therapy. This construct had better water solubility and pharmacokinetics than IR808 and had similar photophysical properties, tumor targeting ability, and photothermal anticancer effect to IR808. By a simple labeling process, IR808-DOTA was labeled with gallium-68 and applied as a PET probe for tumor imaging in MCF-7 tumor xenografted mice. IR808-DOTA itself acted as an NIRF imaging agent in the following surgery for intraoperative navigation to aid surgeons in the delineation of tumor margins and visualizing sentinel lymph nodes to facilitate a more thorough tumor resection. Irradiation by laser, IR808-DOTA could prominently inhibit tumor growth in MCF-7 subcutaneous tumor model mice by directly ablating tumor cells, inhibiting tumor proliferation, and promoting tumor cell apoptosis. In summary, <sup>68</sup>Ga-DOTA-IR808 could enable a convenient and user-friendly workflow for tumor imaging and guided surgery, and therefore, it may have great prospects for clinical translation as a PET/NIRF dual-modal probe.



## 1. INTRODUCTION

Diverse imaging modalities have been extensively used for tumor diagnosis and treatment, including positron emission tomography-computed tomography (PET/CT), magnetic resonance imaging (MRI), and fluorescence molecular imaging (FMI). Each has its advantages and disadvantages for various physiological parameters. To provide more comprehensive physiological and pathological information in a real-time, precise, and specific manner, multimodal imaging has emerged for taking advantage of different imaging modalities, thus greatly improving the efficiency of tumor diagnosis.<sup>1–3</sup> Among them, the complementary nature of PET and near-infrared fluorescence (NIRF) imaging makes the development of strategies for the dual-modal PET/NIRF imaging of cancer a very enticing prospect.<sup>4,5</sup>

For its high tissue penetration and noninvasive properties, PET is used as a reference for preoperative imaging to provide anatomical or metabolism information on tumors.<sup>6–8</sup> However, it is unsuited for real-time intraoperative imaging due to low spatial resolution and short half-life.<sup>9</sup> On the contrary, NIRF imaging has the merits of high spatial and temporal

resolution<sup>10</sup> but has the drawbacks of poor quantification capability and insufficient penetration depth.<sup>11</sup> The complementary nature of these two modalities has led to several preclinical investigations. For instance, PET is applied to the precise preoperative evaluation of cancers. If surgery does occur, NIRF imaging is used for intraoperative navigation to aid surgeons in the delineation of tumor margins, visualizing small metastases and sentinel lymph nodes to facilitate the more thorough tumor resection.<sup>12,13</sup>

In the context of PET/NIRF imaging, it is necessary to develop dual-modal probes for expanding the applicability of this imaging system. <sup>68</sup>Ga-IRDye800CW-BBN (NCT 02910804)<sup>14</sup> and <sup>124</sup>I-cRGDY-PEG-Cdots (NCT01266096)<sup>15</sup> have achieved encouraging results in clinical trials in the field

**Received:** December 28, 2022

**Accepted:** January 19, 2023

**Published:** February 3, 2023



of surgery for glioblastoma and metastatic melanoma.  $^{89}\text{Zr}$ -DFO-ICAM-1-IR800,<sup>16</sup>  $^{89}\text{Zr}$ -ss-dual-5B1,<sup>17</sup> as well as many other PET/NIRF immunoconjugates have been well studied for cancer imaging. Different from multimodal immunoconjugates which image specific tumor types, the heptamethine dyes have aroused general interest as promising PET/NIRF probes for their universal tumor-targeting properties, as well as excellent optical characteristics.<sup>18,19</sup> Through transmembrane proteins of the organic anion transporting polypeptides (OATPs) which are overexpressed in most types of cancer cells in response to hypoxic conditions,<sup>20</sup> certain heptamethine carbocyanine dyes, for instance, IR-780 and its analog IR808, could be transported and show structurally inherent pan-tumor targeting.<sup>19,21</sup> Furthermore, IR808 has excellent absorption in the NIR region, good tissue penetration, low biotoxicity, and superior biocompatibility.<sup>22</sup> Combined with its photothermal heating ability,<sup>23</sup> the potential application scenarios of IR808 in various tumor types are becoming more extensive and interesting. After intraoperative real-time visual evaluation of the three-dimensional relationship between tumors and deep tissues, photothermal therapy can be used as an adjunct therapy to ablate lesions at risk sites (such as paraaortic and vital functional areas of the central nervous system) that cannot be completely resected.

Because the tumor-targeting component is separate from the detection component, traditional dual-mode probes require at least three components, even nanoplatforms. Fortunately, the IR808-based bimodal probe is very easy to develop because IR808 can play the role of the targeting group, the therapeutic group, and the imaging group at the same time. For dual-mode probes intended for intraoperative navigation, the short half-life of gallium-68 protects both the physician and the patient from radiation doses during surgery. Compared with other radionuclides, gallium-68 is an ideal and readily available positron-emitting radionuclide for radiopharmaceutical synthesis.<sup>24</sup> Its chelating procedure with metal chelating agent DOTA is simple and fast with a high radiochemical yield. Therefore, the aim of this study was to couple IR808 with DOTA and then link with gallium-68 to develop a PET/NIRF bimodal probe and evaluate its tumor targeting, photothermal therapeutic properties, and intraoperative navigation ability.

## 2. MATERIALS AND METHODS

**2.1. Synthesis of IR808-DOTA.** IR808 (1-(5-Carboxypentyl)-2-[2-[3-[[1-(5-carboxypentyl)-1,3-dihydro-3,3-dimethyl-2H-indol-2-ylidene]ethylidene]-2-chloro-1-cyclohexen-1-yl]ethenyl]-3,3-dimethyl-3H-indolium bromide) was purchased from HEOWNS (Tianjin, China) and conjugated with 1,4,7,10-tetraazacyclododecane-1,4,7,10-tetraacetic acid (DOTA) using standard Fmoc chemistry. Steps are as follows: ① Resin preparation: to the CTC resin (0.5 mmol, 1.00 eq, Sub 1.00 mmol/g) and Fmoc-Lys (Dde)-OH (1.50 eq), DIEA (3.00 eq) in DCM (5.00 mL) was agitated with  $\text{N}_2$  for 2 h. ② Deprotection: 20% piperidine in DMF (10.0 mL) was added and agitated the resin with  $\text{N}_2$  for another 30 min. ③ Coupling: A solution of DOTA (3tBu) (2.00 eq), HOAT (2.00 eq), and DIC (2.00 eq) in DMF (5.00 mL) was added to the resin and agitated with  $\text{N}_2$  for 60 min. ④ Deprotection: 2%  $\text{NH}_2\text{NH}_2$  in DMF (20.0 mL) was added and agitated the resin with  $\text{N}_2$  for another 30 min. ⑤ Coupling: A solution of 6-(2-((E)-2-((E)-3-((E)-2-(1-(5-carboxypentyl)-3,3-dimethylindolin-2-ylidene)ethylidene)-2-chlorocyclohex-1-en-1-yl)vinyl)-3,3-dimethyl-3H-indol-1-ium-1-yl)hexanoate (1.00 eq),

HOAT (1.50 eq), and DIC (1.50 eq) in DMF (10.0 mL) was added to the resin and agitated with  $\text{N}_2$  for 60 min. ⑥ Cleavage and purification: the resin was washed with MeOH (100 mL\*3) and dried under vacuum to get 1.3 g peptide resin. The peptide is precipitated with cold isopropyl ether and centrifuged and washed two times with isopropyl ether. The residue was purified by prep-HPLC (A: 0.075% TFA in  $\text{H}_2\text{O}$ , B: ACN) to give the final product IR808-DOTA which was confirmed by liquid chromatography–mass spectroscopy (LC–MS) ( $R_t = 1.686$  min) and high-performance liquid chromatography (HPLC). The synthesis scheme is shown in Figure S1.

**2.2. Characterization of IR808-DOTA.** The UV/vis absorption spectra of IR808-DOTA were obtained using a UV/vis spectrophotometer (UV-1601PC, Shimadzu, Japan). The emission spectra were recorded using a fluorescence spectrometer (Edinburgh Instruments FSS, UK).

To evaluate the photothermal efficiency of IR808-DOTA in vitro, IR808-DOTA (containing 0, 50, 100, and 150  $\mu\text{g}/\text{mL}$  of IR808) solution was irradiated using an 808 nm wavelength laser power (1  $\text{W}/\text{cm}^2$ ) for 0–180 s. The temperature changes of each group were recorded by an infrared thermal camera (E8xt, FLIR System Inc., USA). To measure the photothermal efficiency, IR808-DOTA (100  $\mu\text{g}/\text{mL}$ ) was exposed to laser irradiation for 0–180 s with different laser powers (0.5, 1.0, 1.5, 2.0  $\text{W}/\text{cm}^2$ ).

To compare the fluorescence intensity of IR808-DOTA and IR808 at the same excitation wavelength in vitro, IR808 and IR808-DOTA with different concentrations were poured into a 96-well plate and imaged by the Lago X optical imaging system (Spectral Instrument Imaging, Tucson, Arizona USA).

**2.3. Radiolabeling of  $^{68}\text{Ga}$ -DOTA-IR808.** In brief, 10  $\mu\text{L}$  of IR808-DOTA (1  $\mu\text{g}/\mu\text{L}$ , dissolved in ultrapure water) was mixed with 250  $\mu\text{L}$  of sodium acetate buffer (0.25 M). Then, radiolabeling was accomplished by the addition of 1 mL of  $^{68}\text{GaCl}_3$  (0.05 M hydrochloric acid as eluant, 100~200 MBq) obtained from a commercial  $^{68}\text{Ge}/^{68}\text{Ga}$  generator (Isotope Technologies Garching GmbH, Garching, Germany). After heat shock at 95  $^\circ\text{C}$  for 10 min, the mixture was purified by Sep-Pak C-18 (Waters Corporation, Milford, MA, USA). Free  $^{68}\text{Ga}$  was diluted with 5 mL of deionized water, and the desired  $^{68}\text{Ga}$ -DOTA-IR808 was eluted with 500  $\mu\text{L}$  of 95% ethanol. Radiochemical purity and yield were tested using radio high-performance liquid chromatography (radio-HPLC, Waters Corporation) equipped with a 1525 Binary Pump, a 2489 UV/visible detector, an FC-3200 flow count radiation detector (Eckert & Ziegler, Germany), and a 4.6  $\times$  250 mm Luna C18 HPLC column (Phenomenex, CA, USA). The solvent system was a gradient of  $\text{H}_2\text{O}$  with 0.1% TFA (A) and acetonitrile (B): flow rate 1.0 mL/min; 0–5 min 95% A/5% B; 5–10 min 95% A/5% B to 5% A/95% B; 10–15 min 5% A/95% B; 15–20 min 5% A/95% B to 95% A/5% B.

**2.4. Stability and Partition Coefficient of  $^{68}\text{Ga}$ -DOTA-IR808.** The in vitro stability of  $^{68}\text{Ga}$ -DOTA-IR808 was determined by incubation in saline or serum at 37  $^\circ\text{C}$  for 2 to 4 h. For the serum mixture, plasma protein in the incubated solution was precipitated by adding 0.5 mL of anhydrous acetonitrile, followed by centrifugation at 12,000 g for 10 min. The supernatant was then analyzed by radio-HPLC. The in vivo metabolic stability was determined by the injection of  $^{68}\text{Ga}$ -DOTA-IR808 (74 MBq) into BALB/c nude mice (female, 6–8 w, 20–22 g, Charles River, Beijing, China). At

2 and 4 h p.i., mouse urine was collected and its radiochemical purity was identified using radio-HPLC.

For determining the oil–water partition coefficient,  $^{68}\text{Ga}$ -DOTA-IR808 was dissolved in a mixture of water and n-octanol (1:1 ratio V/V) at room temperature, followed by sonication for 10 min. Radioactivity was measured using a gamma counter (PerkinElmer WIZARD2 2470, Shelton, CT, USA). The partition coefficient was expressed as  $\text{Log}P = \log_{10} \left[ \frac{\text{radioactivity in octanol}}{\text{radioactivity in water}} \right]$ .

**2.5. Cell Uptake Assay.** MCF-7 cells ( $1 \times 10^5$ /well) were incubated with IR808-DOTA at an increasing concentration from 1 to 5  $\mu\text{g}/\text{mL}$  for 1 h, followed by a thorough wash. Cells were then measured by flow cytometry (FACSVerse; BD Biosciences, CA, USA) and the intensity of IR808-DOTA fluorescence was analyzed using FlowJo software (Flow Jo, LLC, Ashland, OR, USA). To evaluate the uptake of radiolabeled IR808-DOTA, cells were cultured in a medium supplemented with 0.074 MBq  $^{68}\text{Ga}$ -DOTA-IR808 for 15–120 min. After thorough washes, cells were lysed using 0.1 M NaOH and the radioactivity of lysates was measured by a gamma counter. OATPs inhibitor bromosulfophthalein (BSP, 500  $\mu\text{M}$ , MedChemExpress, New Jersey, USA) preconditioned cells were treated the same as the block group. The nontumorigenic epithelial breast cell line MCF-10A was set as a negative control. MCF-7 and MCF-10A cells were originally obtained from American Type Culture Collection (ATCC). MCF-7 and MCF-10A cells were cultured in DMEM containing 10% fetal bovine serum (Gibco, NY, USA) or MCF-10A cell special media (Procell, Wuhan, China), respectively.

**2.6. Cytotoxicity Assay.** MCF-7 ( $4 \times 10^4$ /well) cells were cultured with IR808-DOTA or IR808 at different concentrations for 24 h, then with/without 808 nm laser irradiation (1 W/cm<sup>2</sup>) for 10 min. PBS-treated cells were set as the blank control. Cell viability was assayed by a CCK-8 kit (Beyotime, Shanghai, China) according to the manufacturer's recommendation. The absorbance was measured at 450 nm using a microplate reader (Biotek Synergy H1, USA). Cell viability was expressed as  $\text{Cell viability} = \frac{\text{OD}_{\text{treated}} - \text{OD}_{\text{blank}}}{\text{OD}_{\text{control}} - \text{OD}_{\text{blank}}} \times 100\%$ . Triplicates were set.

**2.7. Establishment of the Tumor-Bearing Mice Model.** To establish the subcutaneous tumor xenograft model,  $1 \times 10^6$  MCF-7 cells were subcutaneously inoculated into the shoulders of BALB/c nude mice. When the tumor volumes reached 50–100 mm<sup>3</sup>, mice were treated as follows. All the athymic female nude BALB/c mice were purchased from Charles River (Beijing, China), and the weight of each mouse was 20–22 g. All animal protocols were approved by the Experimental Animal Welfare Ethics Committee, Zhongnan Hospital of Wuhan University.

**2.8. Fluorescence Imaging.** All the NIRF images were captured using the Lago X optical imaging system at certain parameters ( $\lambda_{\text{ex}} = 770$  nm,  $\lambda_{\text{em}} = 810$  nm, binning = 1, exposure time = 20 s). For whole-body imaging, MCF-7 tumor-bearing mice were imaged after intravenous injection with IR808-DOTA or IR808 (20  $\mu\text{g}/\text{mouse}$ ) for 6, 24, 48, and 72 h. The intensities of the fluorescence signal were measured by drawing the regions of interest (ROIs) on the whole body or tumors and normalized by subtracting the background ROIs recorded from the other mice with PBS injection using Living Image software. All mice were anesthetized with isoflurane during imaging. Mice were sacrificed and the tissues of interest were collected after imaging (6, 24, and 72 h time points). The

real-time distributions of fluorescence in isolated tissues were carried out immediately. Fluorescent intensities were analyzed by drawing the ROIs on each organ and normalized to tumor volumes. For tumor tissue imaging, dissected tumors were fixed in formalin for a frozen section. Then, fluorescence scanning was performed under a fluorescence microscope.

**2.9. Small Animal PET/CT Imaging and Radiobiodistribution.** Two days after modeling, mice were injected with  $^{68}\text{Ga}$ -DOTA-IR808 (7.4 MBq, 100  $\mu\text{L}$ ) and a ten-minute static PET scan was acquired at 15, 30, 60, 120, 240, and 360 min post-injection. Image data were reconstructed after attenuation correction. ROIs were drawn on the attenuation-corrected image to calculate the percentage injected dose per gram tissue (%ID/g) of the tumor and muscle. A time-uptake curve of the tumor was established accordingly. For the blocking group, mice were pretreated with 500-fold excess IR808 30 min before the radiotracer injection. PET scans were conducted using a micro-PET/CT (Beijing Yongxin Medical Equipment Co., Ltd., Beijing, China). All mice were anesthetized with isoflurane during imaging.

For the radiobiodistribution study, tumor-bearing mice were injected with 3.7 MBq  $^{68}\text{Ga}$ -DOTA-IR808. After 0.5 to 4 h, mice were sacrificed, and main organs and tumors were dissected, weighed, and analyzed. The radioactivity of each sample was normalized for injected dose and organ/tissue weight and expressed as %ID/g.

**2.10. Image-Guided Surgery and Lymphatic Mapping.** For image-guided surgery, 48 h after intravenous injection of IR808-DOTA (100  $\mu\text{L}$ , 10  $\mu\text{g}$ ) into tumor-bearing nude mice, tumor resection was guided by NIRF imaging.

For lymphatic mapping, tumor-bearing mice were intradermally injected with IR808-DOTA (10  $\mu\text{L}$ , 1  $\mu\text{g}$ ) on the hind footpad. Lymphatic drainage and sentinel lymph node imaging were carried out 30 min later.

**2.11. In Vivo Photothermal Therapy for Tumor.** The modeling mice were divided into IR808-DOTA, IR808, or PBS-treated groups. They were injected with IR808-DOTA, IR808 (150  $\mu\text{L}$ , 5 mg/kg per mouse), or the same volume of PBS. Twenty-four hours later, mice were irradiated with/without NIR laser (1 W/cm<sup>2</sup>, 10 min). The temperature changes of tumor tissues were monitored immediately and completed within 600 s using an infrared thermal camera. Tumor diameters and the weights of mice were recorded every two days. The mice were photographed 0, 4, and 14 days after treatment.

**2.12. Hematoxylin and Eosin Staining and Immunostaining.** Mice were sacrificed after photothermal therapy. Serial longitudinal paraffin sections (10  $\mu\text{m}$  thick) were prepared from tumor and organ tissue wax blocks. Sections were stained with HE to detect the morphology. Tumor sections were further immunostained with anti-Ki67 mAb (Biossci Wuhan, China) and anti-HSP70 mAb (Abcam, CA, USA). The TUNEL assay was carried out according to the manufacturer's recommendation (Biossci).

**2.13. Statistical Analysis.** All statistical analyses were performed using GraphPad Prism (version 8.0.2). Data were expressed as mean  $\pm$  standard deviation. Differences between the two groups were analyzed by the *t* test. A *P*-value < 0.05 was considered statistically significant.

## 3. RESULTS

**3.1. IR808-DOTA Retains Superb Photophysical Properties.** IR808 was conjugated with DOTA to yield

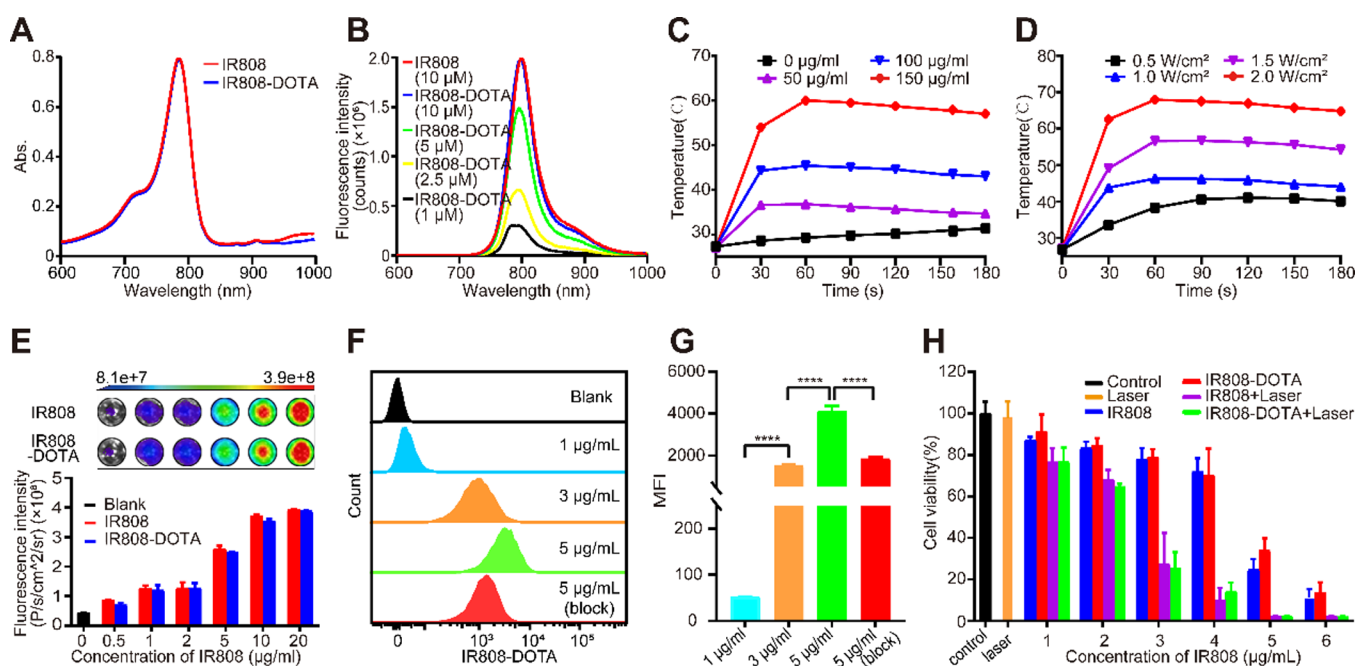


**Figure 1.** Properties of IR808-DOTA. (A) Absorbance and (B) emission spectrum of IR808-DOTA and IR808 in H<sub>2</sub>O. Photothermal heating abilities of IR808-DOTA at different concentrations (808 nm, 1 W/cm<sup>2</sup> for 3 min) (C) and variable irradiation power densities at a concentration of 100 µg/mL (D). Distilled water was used as a negative control. (E) NIRF images of IR808-DOTA and IR808 at indicated concentrations (upper) and images based on quantitative analysis (lower). (F) Concentration-dependent accumulation of IR808-DOTA in MCF-7 cells detected by flow cytometry. For the blocking study, cells were pre-treated with 500 µM BSP for 30 min before incubation with IR808-DOTA. (G) FCM-based quantitative analysis of uptake. (H) Cell viabilities of MCF-7 cells treated by IR808 or IR808-DOTA with/without NIR (808 nm, 1 W/cm<sup>2</sup>, 10 min) irradiation at indicated concentrations. \*\*\*\**P* < 0.0001.

IR808-DOTA according to the synthesis scheme shown in Figure S1. The chemical composition of IR808-DOTA was confirmed by HPLC (Figure S2A) and mass spectrometry (calcd 1197.8) (Figure S2B). UV absorbance of the compound was analyzed and compared with IR808, demonstrating an optimal maximum absorption peak at 776 nm and no peak shift in the case of the compound (Figure 1A). In addition, the fluorescence spectrometer analysis indicated that the optimal maximum emission peak of the compound occurred at ~800 nm (Figure 1B), which was similar to that of IR808.

To evaluate the photothermal property, the compound was irradiated with laser. Results manifested that IR808-DOTA showed dose-dependent and power-density-dependent photothermal heating ability. Even in a low laser density of 1 W/cm<sup>2</sup> 808 nm at a concentration of 100 µg/mL, the temperature could reach 44.3 °C within 30 s (Figure 1C,D). NIR fluorescence imaging was observed in the optical imaging system for IR808-DOTA solution and IR808 solution (Figure 1E). The fluorescence signals of the two samples were enhanced gradually with the increase of the solution concentration, and the fluorescence intensity of the two groups was similar at the same concentration. FCM also showed that the IR808-DOTA was uptaken by cells in a dose-dependent manner. The inhibitor (BSP) of OATPs, which mediates tumor uptake preference of IR808, could reverse the accumulation of IR808-DOTA in tumor cells (Figure 1F,G). Consistent with the photothermal heating ability, IR808-DOTA-treated cells lost their viability in a dose-dependent way when exposed to laser irradiation. The cytotoxicity and phototoxicity of IR808-DOTA to cells were not significantly different from those of IR808 (Figure 1H).

The above data indicated that the photophysical properties of IR808 were not impaired by coupling with DOTA.

**3.2. IR808-DOTA Shows Strong Tumor-Targeting Ability In Vivo.** NIRF images from MCF-7 tumor-bearing mice injected intravenously with IR808-DOTA (Figure 2A) showed that the fluorescence signals were observed in the tumor tissues at 6 h post-injection, reaching the brightest at 24 h and then declining slowly. Even at 72 h post-injection, fluorescence signals in the tumor could also be visible while almost being cleared away from normal tissues. The variation trend of the IR808-DOTA signal in the tumor tissues was consistent with that of IR808 under the same conditions (Figure 2B). Different from its tumor-targeted accumulation, IR808-DOTA was gently uptaken by the normal tissue (ear) within the first 6 h and then was cleared away steadily (Figure 2C). Frozen sections from resected tumors showed the even distribution of IR808-DOTA red fluorescence in tissues (Figure 2D). The isolated tissues image (Figure 2E–G) showed that fluorescence accumulated in tumors at 6 h and peaked at 24 h post-injection. Except for tumors, IR808-DOTA is also mainly distributed in the kidney, liver, and lungs. At 72 h, signals were cleared away from those organs. Drug clearance was observed to be slower in the tumor than in other tissues.

These data suggested that IR808-DOTA was preferentially uptaken by tumors and retained for a long time, with a good target-to-nontarget ratio.

**3.3. <sup>68</sup>Ga-Labeled IR808-DOTA Is a Feasible PET Radiotracer for Tumor Imaging.** To detect whether IR808-DOTA could be developed as a NIR heptamethine dye-based PET probe that enables gross navigation of deep-tissue organs and determination of disease extent in vivo,

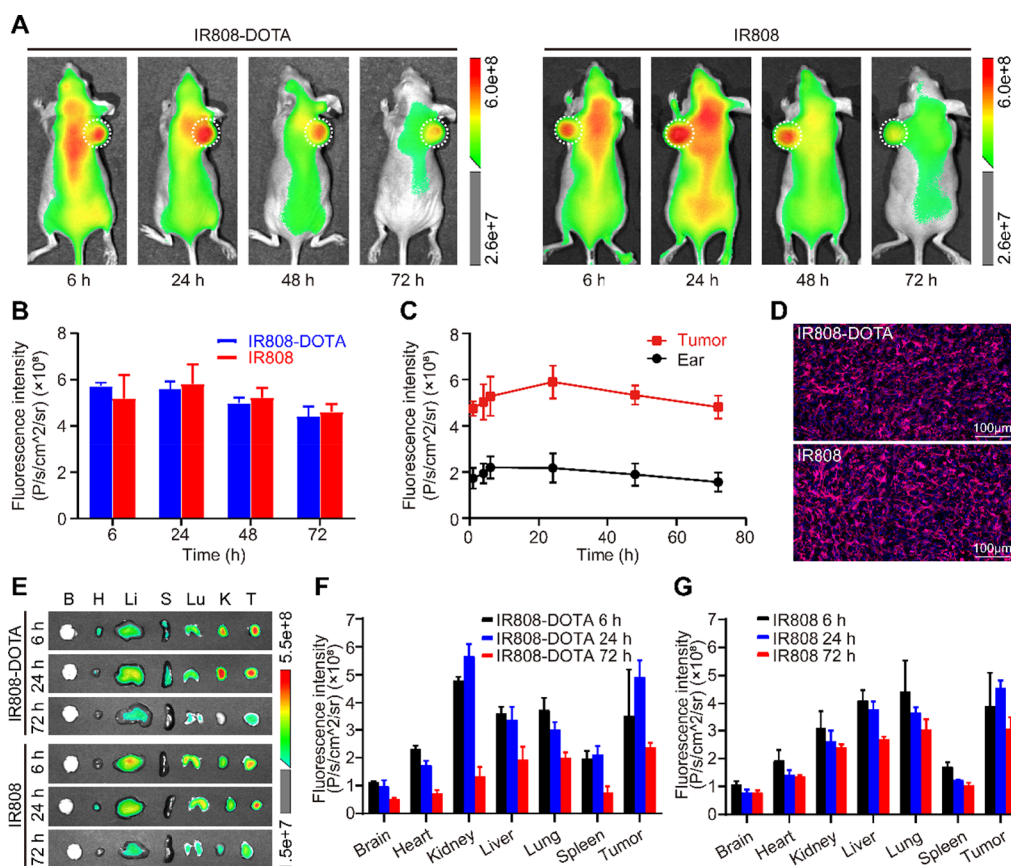


**Figure 2.** Tumor-targeting evaluation of IR808-DOTA by fluorescence imaging. (A) Representative NIR fluorescence images of MCF-7 tumor-bearing mice at indicated time points after a single intravenous injection of IR808-DOTA or IR808 (20  $\mu\text{g}/\text{mouse}$ ). White dotted circles point to tumors. (B,C) Intensities of the fluorescence signal of tumors and normal tissue (ear) of mice were measured by drawing the ROIs using Aura Image Analysis Software v3.2 ( $n = 3$ ). (D) Fluorescence distribution in tumor sections, 24 h p.i. (E) Representative NIR fluorescence images showed the distribution of IR808-DOTA and IR808 in vital dissected organs and tumors (B, brain; H, heart; Li, liver; S, spleen; Lu, lung; K, kidney; T, Tumor). Fluorescence intensity-based quantitative analysis of IR808-DOTA (F) and IR808 (G) uptake in organs and tumors ( $n = 3/\text{group}$ ).

IR808-DOTA was labeled with  $^{68}\text{Ga}$  by one step. Results showed that, by this simplified process,  $^{68}\text{Ga}$ -DOTA-IR808 was prepared with >95% radiochemical yield and with >99% radiochemical purity. The molar activities of the radiotracer were 14.8–37.0 MBq/nmol. It exhibited excellent in vitro and in vivo metabolic stability (Figure 3A). The logP value of  $^{68}\text{Ga}$ -DOTA-IR808 was  $-1.65 \pm 0.03$  ( $n = 4$ ). The following in vitro tumor targeting analysis (Figure 3B) showed that  $^{68}\text{Ga}$ -DOTA-IR808 was highly accumulated in MCF-7 cells but lowly in nontumorigenic MCF-10A cells. MCF-7 cells had three times as much probe uptake as MCF-10A cells ( $P < 0.01$ ). The OATP inhibitor BSP significantly inhibited the uptake in MCF-7 cells ( $P < 0.05$ ).

PET images were collected at 15, 30, 60, 120, 240, and 360 min after the administration of  $^{68}\text{Ga}$ -DOTA-IR808 (Figure 3C). The images acquired at the earliest time point (15 min) clearly illustrated that this  $^{68}\text{Ga}$ -labeled NIRF dye was capable of the rapid and high-contrast visualization of the tumor tissue. The background of the images improved over time, and the agents gradually concentrated in the tumors. Image-based quantitative analysis confirmed that  $^{68}\text{Ga}$ -DOTA-IR808 accumulated in tumor tissues rapidly while declining regularly in the muscle within 6 h (Figure 3D). The ratio of tumor-to-normal tissue (T/M: tumor/muscle) increased rapidly and was even greater than 8 at a 360 min time point (Figure 3E).

Pretreatment with an excess of unlabeled IR808 could evidently block the accumulation of the radiotracer in tumor tissues (Figure 3C,F).

Biodistribution experiments mirrored the observations made during PET imaging (Figure 3G, Table S1). At 0.5 h post-injection, the activity concentration in the tumor was  $1.13 \pm 0.21$  %ID/g, a value which grew to  $3.21 \pm 0.67$  %ID/g by 4 h. Various healthy organs, including the brain, heart, stomach, bone, intestine, and spleen, had activity concentrations below 2 %ID/g within 4 h post-injection. At 4 h p.i., the blood pool and kidney were the nontarget sites with the highest activity concentrations, inferring the renal elimination of excess IR808-DOTA. Since the observation of the long-term distribution of IR808-DOTA was limited by the short half-life of  $^{68}\text{Ga}$ , it was complemented by the fluorescence distribution shown in Figure 2F. In those long-term observations, IR808-DOTA accumulation in tumors peaked at 24 h pi, which was consistent with the previous results of fluorescence imaging. In addition, IR808-DOTA signals in the kidney at 6 and 24 h pi were much higher than IR808 signals for which the liver was the predominant nontarget organ throughout the observation period, suggesting a slight shift from liver metabolism to renal excretion of IR808 after conjugation with DOTA.

**3.4. IR808-DOTA-Based NIRF Imaging Guides Intraoperative Surgery.** The PET and biodistribution results

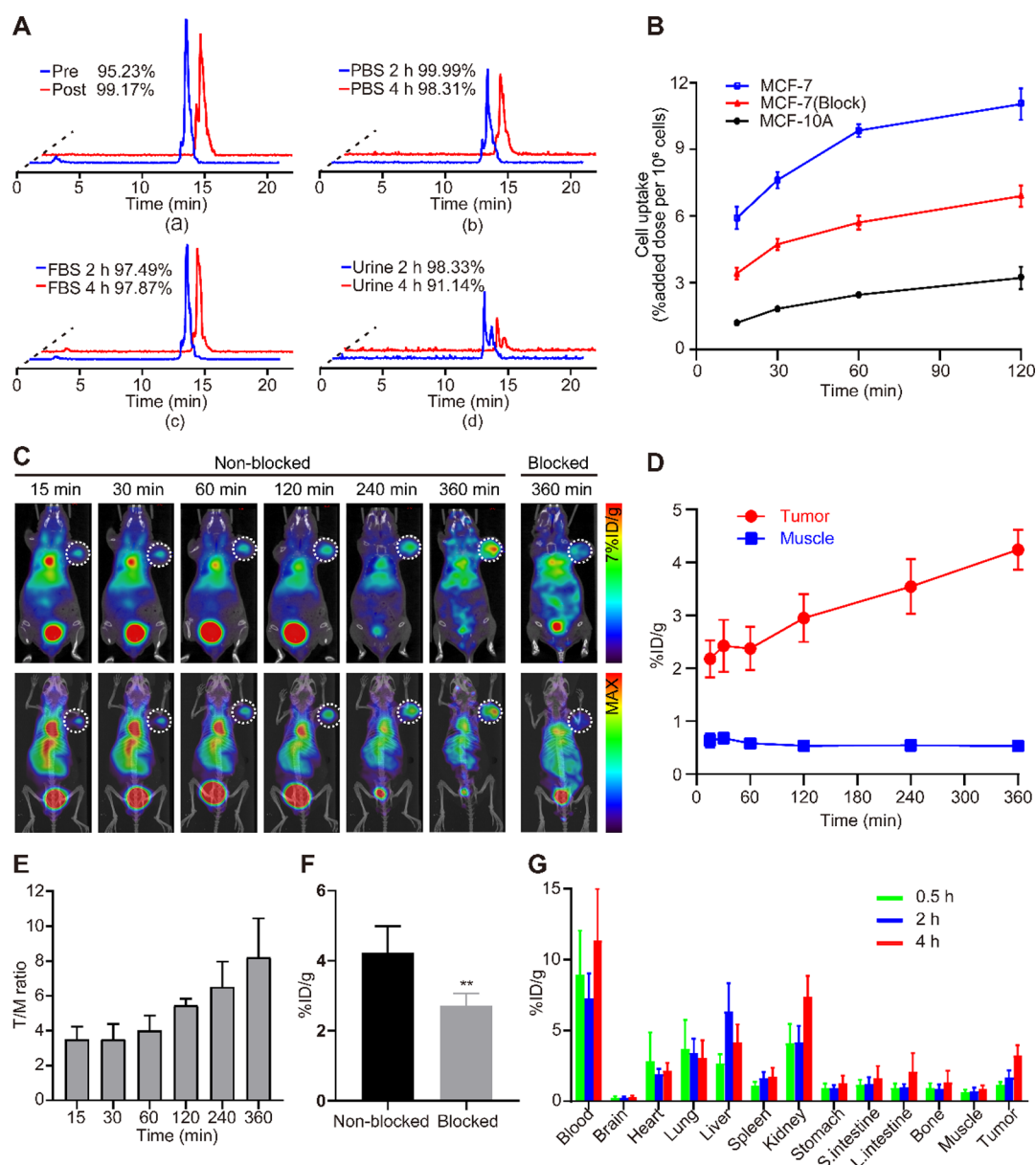


**Figure 3.** Properties and tumor-targeting evaluation of  $^{68}\text{Ga}$ -DOTA-IR808. (A-a) Analytical radio-HPLC profiles of  $^{68}\text{Ga}$ -DOTA-IR808 before (blue) and after purification (red). In vitro stability of  $^{68}\text{Ga}$ -DOTA-IR808 in PBS (A-b) and FBS (A-c), respectively, 2 and 4 h after incubation. (A-d) In vivo stability of  $^{68}\text{Ga}$ -DOTA-IR808 in the urine of mouse 2 and 4 h p.i. (B) Uptake of  $^{68}\text{Ga}$ -DOTA-IR808 by MCF-7 and MCF-10A cells using a gamma counter. OATP inhibitor BSP was used for blocking. (C) Representative PET/CT images of MCF-7 tumor-bearing mice at different time intervals (15, 30, 60, 120, 240, and 360 min) after the injection of  $^{68}\text{Ga}$ -DOTA-IR808. IR808 was injected by the tail vein before the administration of  $^{68}\text{Ga}$ -DOTA-IR808 as a competitive blocker. White dotted circles indicate tumors.  $n = 5$ . (D) PET images based on the quantitative analysis of  $^{68}\text{Ga}$ -DOTA-IR808 uptake in tumor and normal tissue (muscle) of mice. (E) Time-tumor/muscle (T/M) ratio curves. (F) Comparison of  $^{68}\text{Ga}$ -DOTA-IR808 uptake in tumors before and after the blockade. A 500-fold excess of unlabeled IR808 was used for blocking. (G) Biodistribution of  $^{68}\text{Ga}$ -DOTA-IR808 in mice, 0.5, 2, and 4 h p.i. ( $n = 5$ /group).  $**P < 0.01$ .

strongly suggested that IR808-DOTA-based PET/NIRF imaging could be highly effective for the image-guided resection of the tumor tissue. To explore this possibility, NIRF imaging was performed on the mice of the PET imaging cohort. The in vivo fluorescence images clearly illustrated the specific localization of IR808-DOTA to the subcutaneous MCF-7 tumor xenografts. Nodular in situ was successfully removed through simulated resection, which was well reflected in the displacement of sharp signals and the H&E-stained section of the resected tissue (Figure 4A,B). In the process of fluorescence-guided tumor resection, a deeper small lesion with fluorescence-emitting signals was found and removed,

which was confirmed as lymph node metastasis by H&E staining (Figure 4B).

For lymphocyte mapping, IR808-DOTA was injected into the left hind paw of mice. Thirty minutes later, NIRF images clearly showed that the fluorescence signal traveled along the lymphatic vessels from the injection site and aggregated to the popliteal and sacral lymph nodes (Figure 4C).

These results enable the IR808-DOTA-based NIRF-guided excision of the tumor tissue and metastatic lymph nodes.

**3.5. IR808-DOTA Shows Strong Photothermal Anti-Cancer Efficacy.** Based on the above data indicating that IR808-DOTA would be feasible for PET/NIRF dual-mode

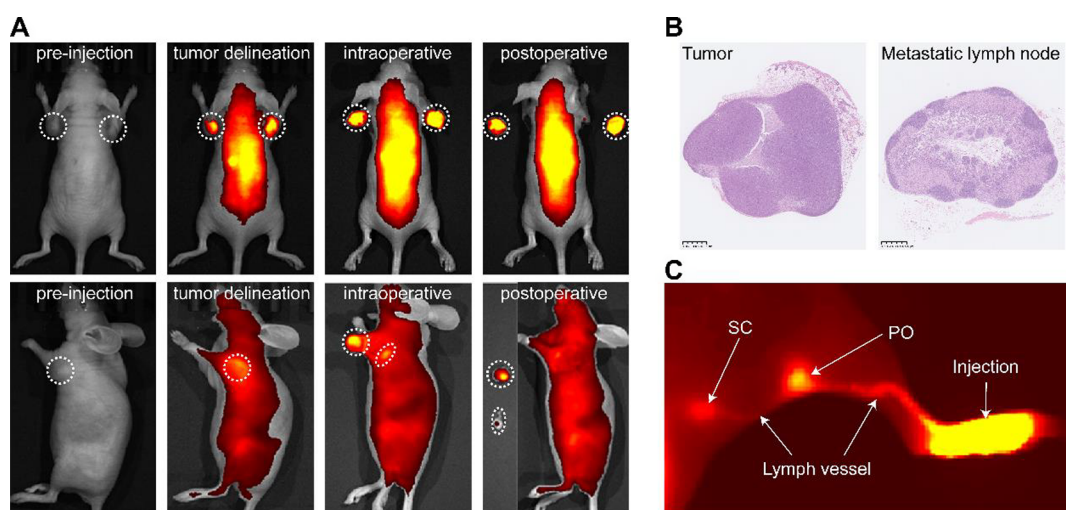


**Figure 4.** Image-guided cancer surgery using IR808-DOTA. (A) With NIRF imaging, tumor mass and metastatic lymph nodes were delineated and resected thoroughly. White dotted circles and oval circles indicated tumor tissues and metastatic lymph nodes, respectively. (B) Representative H&E staining of the resected tumor and metastatic lymph nodes. (C) Lymph node mapping was executed using a hypodermic probe into the footpad. PO: popliteal lymph node; SC: sacral lymph node.

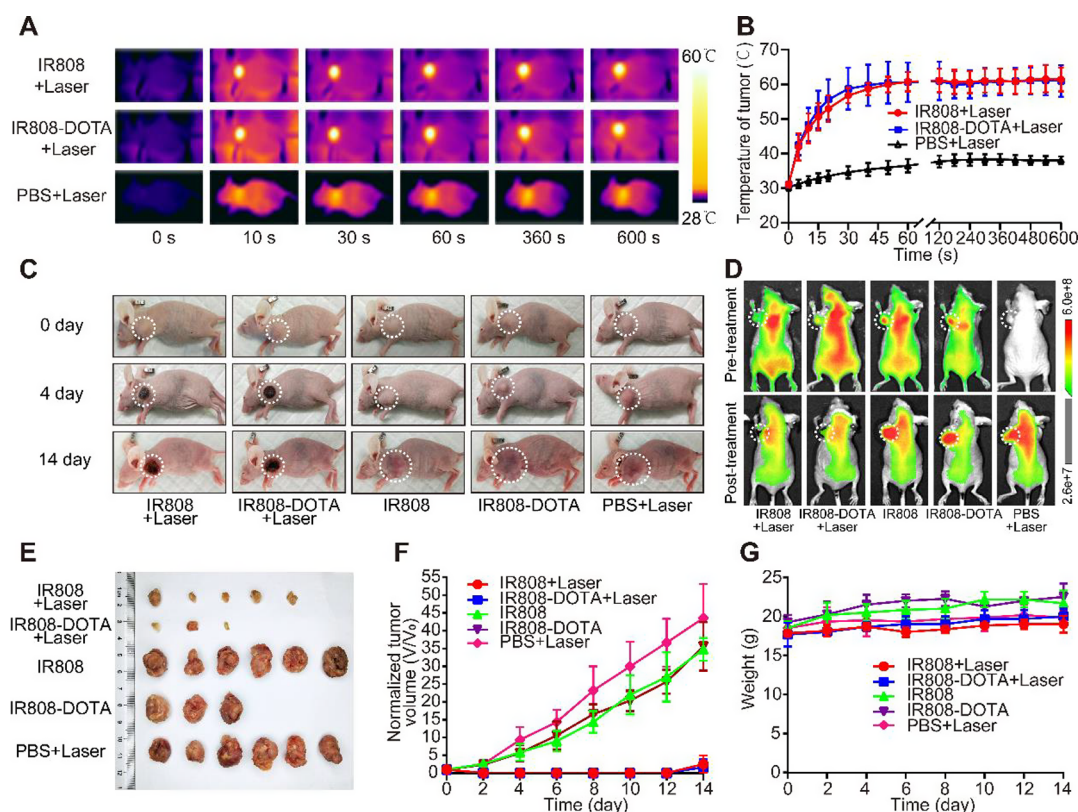


**Figure 5.** Photothermal therapeutic efficacy of IR808-DOTA (containing 5 mg/kg of IR808 per mouse) after photothermal treatment. (A) Temperature increase profiles in MCF7 tumor tissue after in vivo photothermal treatment (808 nm, 1 W/cm<sup>2</sup> for 10 min). Representative infrared thermal images were taken using an infrared thermal camera. (B) Infrared thermal images based on quantitative analysis of temperature increase in tumor tissues. (C) Whole-body images of tumor-bearing mice 0, 4, and 14 days after treatment. (D) Comparison of the tumor size in mice using NIRF imaging before and 14 days after treatment. White dotted circles show tumors. (E) Photographs of tumor tissues. (F) Tumor growth curves. (G) Body weights.  $n = 3-6$ .

imaging, its photothermal application was then conducted. MCF-7 tumor-bearing mice were irradiated at the tumor sites with 808 nm laser (1.0 W/cm<sup>2</sup>, 10 min) 24 h after the injection of IR808-DOTA (Figure 5A). As control, PBS/IR808 injection groups were also included. After 1 min of laser irradiation, the average photothermal temperature in the tumor of mice

treated with IR808-DOTA/IR808 reached approximately 60 °C, which was more than enough for the photothermal ablation of the tumor cells. However, under the same laser irradiation, the average temperature of the tumor treated with PBS only increased by 8 °C at most (Figure 5B). Consistently, after laser irradiation, IR808-DOTA-treated mice presented

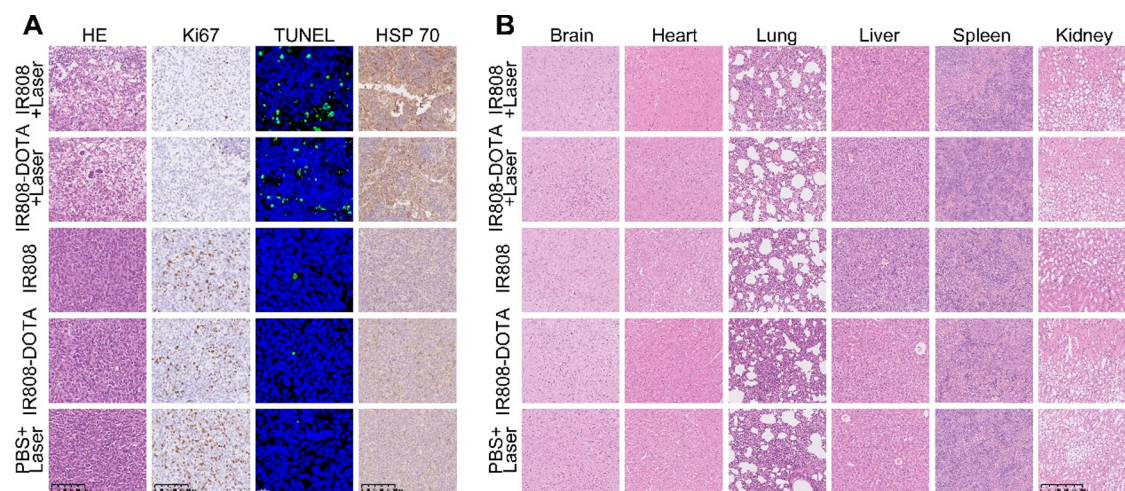


**Figure 6.** (A) H&E and immunostaining for Ki67, TUNEL, and HSP70 in tumor sections. (B) Safety evaluation of photothermal therapy. H&E staining of the major tissues, including the brain, heart, lung, liver, spleen, and kidney. Scale bar, (A) 100  $\mu\text{m}$  (TUNEL, 20  $\mu\text{m}$ ), (B) 250  $\mu\text{m}$ .

obvious bleeding and necrosis at the irradiation sites, leaving black scars at their original sites without showing tumor enlargement at day 14. These phenomena were also observed in IR808-treated mice but not in the PBS treatment group (Figure 5C). Without irradiation, IR808-DOXA and IR808 failed to produce thermal energy to make substantial damage to tumors (Figure 5C). The thermal-based ablation of tumors was also visualized by NIRF imaging (Figure 5D) and resected tumor photographs (Figure 5E) which showed that tumor sizes in IR808-DOXA/IR808-treated mice after laser irradiation were significantly smaller than those in the PBS group or without irradiation. The average tumor volumes in the latter groups at day 14 were over 35 times larger than their initial ones, while in IR808-DOXA/IR808-treated groups, no more than 3 times (Figure 5F). During 14 days of treatment, there was no significant body weight loss in all five groups (Figure 5G).

To further assess the photothermal anti-cancer therapeutic effect of IR808-DOXA, tumor sections were histologically analyzed concerning proliferation, heat-shock response, and signs of apoptosis (Figure 6A). Results manifested that tumor sections from IR808-DOXA plus laser-treated group exhibited the utmost severe coagulation, vacuolation, and disappearance of nuclear staining. The frequencies of its TUNEL-positive cells and HSP70-colored cells were greatly increased while Ki67-positive cells were decreased when compared with those with PBS treatment or without irradiation, suggesting that IR808-DOXA-treated cells responded to heat stress and died by apoptosis.

Finally, the biological safety of IR808-DOXA was evaluated. H&E staining showed that, following IR808-DOXA infusion and laser irradiation, the mice did not develop a progressively worsening disease characterized by significant pathological changes in the major organs, including the brain, heart, lung, liver, spleen, and kidney (Figure 6B). In addition, mice did not lose their body weight during the entire observation period (Figure 5G).

Collectively, these results suggested that IR808-DOXA-based photothermal therapy showed strong anti-cancer efficacy and IR808-DOXA infusion elicited no systemic toxicity to xenografted mice.

#### 4. DISCUSSION

In this study, the precursor IR808-DOXA was successfully synthesized. IR808-DOXA was easily labeled with  $^{68}\text{Ga}$  with a high radiochemical yield and perfect stability. We demonstrated that the coupling changed the lipophilic cationic property of the heptamethine core of IR808 but kept the photophysical properties and tumor-targeting functions. IR808-DOXA has excellent tumor imaging, intraoperative navigation, and imaging-guided photothermal therapy capabilities.

The FCM analysis and the radioactive uptake test demonstrated that coupling with DOTA did not influence the targeting ability of IR808 to tumor cells. The explanation is that the functional group determining the biological activity of IR808 is the rigid cyclohexenyl ring within the methine bridge,<sup>25</sup> which is not a DOTA link modification site. However, coupling with DOTA did influence some properties of IR808, for instance, water solubility, for IR808-DOXA prefers renal excretion rather than liver metabolism. The underlying mechanism is worthy of further investigation for improving the solubility of other related chemicals.

As revealed by the results of the NIRF imaging, IR808-DOXA was maintained in the tumor for at least 72 h post injection, which was beneficial for the development of multifunctional probes with the capacities of tumor intraoperative navigation and photothermal therapy. The signals from PET imaging could be detected at the tumor site as early as 15 min p.i. and would reach their peak at 24 h. Both PET and NIRF imaging enabled the noninvasive visualization of malignant lesions clearly, suggesting that IR808-DOXA was an attractive dual-mode probe that can accurately detect tumors. Biodistribution indicated that in addition to lingering in the tumor, the probe also circulates in the blood pool for a longer period of time with higher radioactive activity, possibly because such tumor-targeting dyes can form covalent compounds with serum albumin.<sup>26</sup> This stable binding mode will be conducive to the application of the probe in intraoperative navigation. After precisely localizing deep tumor lesions by PET imaging, IR808-DOXA-based NIRF imaging successfully guided the excision of tumor tissue and metastatic lymph node, improving cancer surgery outcomes and minimizing anesthesia time. So far, fluorescein (FS),<sup>27</sup> methylene blue (MB),<sup>28</sup> indocyanine

green (ICG),<sup>29</sup> and 5-aminolevulinic acid (5-ALA)<sup>30</sup> have been clinically approved for fluorescence image-guided surgery. However, the results are still far from the high-precision resection of tumors in these trials because these agents do not have tumor-targeting ability. Due to its active pan-tumor targeting capability, real-time precision imaging, and long-term retention at the tumor site, IR808-DOTA would be of great value to help surgeons identify tumor boundaries, micro-metastases, and sentinel lymph nodes during surgery and guide surgical high-precision resection. In terms of sentinel lymph node localization, ICG-<sup>99m</sup>Tc-nanocolloid has achieved remarkable clinical trials results,<sup>31</sup> which inspires us to combine IR808-DOTA with other long-half-life nuclides in future studies to apply radio-guided and fluorescent-guided sentinel lymph node recognition, so as to improve its application value.

On account of the heterogeneity and complexity of tumors, combinatorial therapy is considered to be an effective strategy for tumor elimination.<sup>32</sup> Currently, image-guided PTT has been developed as a glamorous strategy for tumor ablation or intraoperative adjuvant therapy owing to its distinguishable merits, such as noninvasiveness, excellent specificity, effective tumor ablation, and fewer side effects.<sup>33,34</sup> In this study, we verified that the IR808-DOTA had a satisfactory photothermal effect-based cytotoxic ability. As a therapeutic agent having cancer targeting, IR808-DOTA is cytotoxic to cancer cells but spares the normal tissue cells in the major organs. The cytotoxicity of IR808-DOTA might derive from the mitochondrial toxicity of the IR808 moiety which inhibits the normal production of ATP energy and thus inhibits the growth and proliferation of cells directly.<sup>35,36</sup> Combined with its potential as a dual-modal probe, IR808-DOTA can be used as an ideal probe for the integration of diagnosis and treatment to effectively monitor cell death and tumor size during treatment and accurately evaluate the effect of photothermal therapy. Moreover, the therapeutic nuclides (e.g., <sup>177</sup>Lu, <sup>90</sup>Y, <sup>47</sup>Sc, <sup>67</sup>Cu, and <sup>225</sup>Ac) can be linked to IR808-DOTA to perform their radionuclide therapy function to maximize the efficacy of the combination therapy. Therefore, it is our sincere hope that IR808-DOTA-based PTT combined with other therapy options will have better tumor treatment outcomes in future searches. We found that IR808-DOTA also has some limitations, such as nonspecific uptake by the liver and lungs. This uptake could be due to the presence of serum albumin in these blood-rich organs, as previously mentioned. We expect that in future studies, chemical modifications can be used to improve the water solubility and the quantum yield of the probe to obtain a better imaging background and therapeutic effects.

## 5. CONCLUSIONS

In brief, our results revealed that IR808-DOTA has the potential as the PET/NIRF dual-modal probe. It retains superb photophysical properties and shows strong tumor-targeting ability and photothermal anti-cancer efficacy as IR808. By a simplified labeling process, IR808-DOTA could be conveniently labeled with gallium-68 and subsequently was applied as a PET probe for deep tumor imaging in MCF-7 tumor xenografted mice. IR808-DOTA itself acted as a NIRF imaging agent in the following surgery for intraoperative navigation to aid surgeons in the delineation of tumor margins and visualizing sentinel lymph nodes to facilitate the more thorough tumor resection. This tracer is of great translational value as the PET/NIRF probe where it could enable a

convenient and user-friendly workflow for tumor imaging and guided surgery.

## ■ ASSOCIATED CONTENT

### Supporting Information

The Supporting Information is available free of charge at <https://pubs.acs.org/doi/10.1021/acsomega.2c08235>.

Synthesis of IR808-DOTA (Figure S1); HPLC analysis and mass spectrometry (Figure S2); and biodistribution of <sup>68</sup>Ga-DOTA-IR808 in MCF-7 xenograft mice (Table S1) (PDF)

## ■ AUTHOR INFORMATION

### Corresponding Authors

**Ping Lei** – Department of Immunology, School of Basic Medicine, Tongji Medical College, Huazhong University of Science and Technology, Wuhan 430030 Hubei Province, China; Email: [adaleip@hust.edu.cn](mailto:adaleip@hust.edu.cn)

**Yong He** – Department of Nuclear Medicine, Zhongnan Hospital of Wuhan University, Wuhan 430071 Hubei Province, China; [orcid.org/0000-0002-9846-7578](https://orcid.org/0000-0002-9846-7578); Email: [heyong@znhospital.cn](mailto:heyong@znhospital.cn)

### Authors

**Jiaxu Zhu** – Department of Nuclear Medicine, Zhongnan Hospital of Wuhan University, Wuhan 430071 Hubei Province, China

**Yaquin Jiang** – Department of Nuclear Medicine, Zhongnan Hospital of Wuhan University, Wuhan 430071 Hubei Province, China

**Xin Pan** – Department of Nuclear Medicine, Zhongnan Hospital of Wuhan University, Wuhan 430071 Hubei Province, China

**Kui Xu** – Department of Nuclear Medicine, Zhongnan Hospital of Wuhan University, Wuhan 430071 Hubei Province, China

**Wenhao Niu** – Department of Immunology, School of Basic Medicine, Tongji Medical College, Huazhong University of Science and Technology, Wuhan 430030 Hubei Province, China

**Yibing Lv** – Department of Immunology, School of Basic Medicine, Tongji Medical College, Huazhong University of Science and Technology, Wuhan 430030 Hubei Province, China

**Chongjiao Li** – Department of Nuclear Medicine, Zhongnan Hospital of Wuhan University, Wuhan 430071 Hubei Province, China

**Yichun Wang** – Department of Nuclear Medicine, Zhongnan Hospital of Wuhan University, Wuhan 430071 Hubei Province, China

**Zejian Xue** – Department of Nuclear Medicine, Zhongnan Hospital of Wuhan University, Wuhan 430071 Hubei Province, China

Complete contact information is available at: <https://pubs.acs.org/10.1021/acsomega.2c08235>

### Author Contributions

<sup>§</sup>J.Z. and Y.J. contributed equally.

### Notes

The authors declare no competing financial interest.

## ACKNOWLEDGMENTS

This work was supported by the National Natural Science Foundation of China (grant numbers 82171986 & 81871391) and the Improvement Project for Theranostic Ability on Difficulty Miscellaneous Disease (grant number ZLYNXM202007). The authors thank Prof. Xiaoli Lan, Prof. Dawei Jiang, and all the team members at Department of Nuclear Medicine, Union Hospital, Tongji Medical College, Huazhong University of Science and Technology for the support in data acquisition and the facility support.

## REFERENCES

- (1) Weissleder, R. Molecular imaging in cancer. *Science* **2006**, *312*, 1168–1171.
- (2) James, M. L.; Gambhir, S. S. A molecular imaging primer: modalities, imaging agents, and applications. *Physiol. Rev.* **2012**, *92*, 897–965.
- (3) Weissleder, R.; Pittet, M. J. Imaging in the era of molecular oncology. *Nature* **2008**, *452*, 580–589.
- (4) Adumeau, P.; Carnazza, K. E.; Brand, C.; Carlin, S. D.; Reiner, T.; Agnew, B. J.; Lewis, J. S.; Zeglis, B. M. A Pretargeted Approach for the Multimodal PET/NIRF Imaging of Colorectal Cancer. *Theranostics* **2016**, *6*, 2267–2277.
- (5) Privat, M.; Bellay, P. S.; Lescure, R.; Massot, A.; Baffroy, O.; Moreau, M.; Racœur, C.; Marcion, G.; Denat, F.; Beltaieb, A.; et al. Development of an Easily Bioconjugatable Water-Soluble Single-Photon Emission-Computed Tomography/Optical Imaging Bimodal Imaging Probe Based on the aza-BODIPY Fluorophore. *J. Med. Chem.* **2021**, *64*, 11063–11073.
- (6) Phelps, M. E. PET: The merging of biology and imaging into molecular imaging. *J. Nucl. Med.* **2000**, *41*, 661–681.
- (7) Jacobs, A. H.; Li, H.; Winkler, A.; Hilker, R.; Knoess, C.; Rüger, A.; Galldiks, N.; Schaller, B.; Sobesky, J.; Kracht, L.; et al. PET-based molecular imaging in neuroscience. *Eur. J. Nucl. Med. Mol. Imaging* **2003**, *30*, 1051–1065.
- (8) Ozkan, E.; Soydal, C.; Araz, M.; Kir, K. M.; Ibis, E. The role of 18F-FDG PET/CT in detecting colorectal cancer recurrence in patients with elevated CEA levels. *Nucl. Med. Commun.* **2012**, *33*, 395–402.
- (9) Cai, W. B.; Chen, X. Y. Multimodality molecular imaging of tumor angiogenesis. *J. Nucl. Med.* **2008**, *49*, 113S–128S.
- (10) Wang, C.; Wang, Z.; Zhao, T.; Li, Y.; Huang, G.; Sumer, B. D.; Gao, J. Optical molecular imaging for tumor detection and image-guided surgery. *Biomaterials* **2018**, *157*, 62–75.
- (11) Luo, S.; Zhang, E.; Su, Y.; Cheng, T.; Shi, C. A review of NIR dyes in cancer targeting and imaging. *Biomaterials* **2011**, *32*, 7127–7138.
- (12) Newton, A. D.; Predina, J. D.; Shin, M. H.; Frenzel-Sulyok, L. G.; Vollmer, C. M.; Drebin, J. A.; Singhal, S.; Lee, M. K. t. Intraoperative Near-infrared Imaging Can Identify Neoplasms and Aid in Real-time Margin Assessment During Pancreatic Resection. *Ann. Surg.* **2019**, *270*, 12–20.
- (13) Zhang, Z.; He, K.; Chi, C.; Hu, Z.; Tian, J. Intraoperative fluorescence molecular imaging accelerates the coming of precision surgery in China. *Eur. J. Nucl. Med. Mol. Imaging* **2022**, *49*, 2531–2543.
- (14) Li, D.; Zhang, J.; Chi, C.; Xiao, X.; Wang, J.; Lang, L.; Ali, I.; Niu, G.; Zhang, L.; Tian, J.; et al. First-in-human study of PET and optical dual-modality image-guided surgery in glioblastoma using (68)Ga-IRDye800CW-BBN. *Theranostics* **2018**, *8*, 2508–2520.
- (15) Phillips, E.; Penate-Medina, O.; Zanzonico, P. B.; Carvajal, R. D.; Mohan, P.; Ye, Y.; Humm, J.; Goenen, M.; Kalaigian, H.; Schoeder, H.; et al. Clinical translation of an ultrasmall inorganic optical-PET imaging nanoparticle probe. *Sci. Transl. Med.* **2014**, *6*, 260ra149.
- (16) Li, M.; Wei, W.; Barnhart, T. E.; Jiang, D.; Cao, T.; Fan, K.; Engle, J. W.; Liu, J.; Chen, W.; Cai, W. ImmunoPET/NIRF/Cerenkov multimodality imaging of ICAM-1 in pancreatic ductal adenocarcinoma. *Eur. J. Nucl. Med. Mol. Imaging* **2021**, *48*, 2737–2748.
- (17) Houghton, J. L.; Zeglis, B. M.; Abdel-Atti, D.; Aggeler, R.; Sawada, R.; Agnew, B. J.; Scholz, W. W.; Lewis, J. S. Site-specifically labeled CA19.9-targeted immunoconjugates for the PET, NIRF, and multimodal PET/NIRF imaging of pancreatic cancer. *Proc. Natl. Acad. Sci. U. S. A.* **2015**, *112*, 15850–15855.
- (18) Guo, H.; Kommidi, H.; Lekaye, C. C.; Koutcher, J.; Judenhofer, M. S.; Cherry, S. R.; Wu, A. P.; Akin, O.; Souweidane, M. M.; Aras, O.; et al. A near-infrared probe for non-invasively monitoring cerebrospinal fluid flow by (18)F-positron emitting tomography and fluorescence. *EJNMMI Res.* **2020**, *10*, 37.
- (19) Zhao, X.; Zhao, H.; Wang, S.; Fan, Z.; Ma, Y.; Yin, Y.; Wang, W.; Xi, R.; Meng, M. A Tumor-Targeting Near-Infrared Heptamethine Cyanine Photosensitizer with Twisted Molecular Structure for Enhanced Imaging-Guided Cancer Phototherapy. *J. Am. Chem. Soc.* **2021**, *143*, 20828–20836.
- (20) Durmus, S.; van Hoppe, S.; Schinkel, A. H. The impact of Organic Anion-Transporting Polypeptides (OATPs) on disposition and toxicity of antitumor drugs: Insights from knockout and humanized mice. *Drug Resistance Updates* **2016**, *27*, 72–88.
- (21) Zhang, E.; Luo, S.; Tan, X.; Shi, C. Mechanistic study of IR-780 dye as a potential tumor targeting and drug delivery agent. *Biomaterials* **2014**, *35*, 771–778.
- (22) Tan, X.; Luo, S.; Wang, D.; Su, Y.; Cheng, T.; Shi, C. A NIR heptamethine dye with intrinsic cancer targeting, imaging and photosensitizing properties. *Biomaterials* **2012**, *33*, 2230–2239.
- (23) Li, S.; Sun, Z.; Deng, G.; Meng, X.; Li, W.; Ni, D.; Zhang, J.; Gong, P.; Cai, L. Dual-modal imaging-guided highly efficient photothermal therapy using heptamethine cyanine-conjugated hyaluronic acid micelles. *Biomater.* **2017**, *5*, 1122–1129.
- (24) Breeman, W. A.; Verbruggen, A. M. The 68Ge/68Ga generator has high potential, but when can we use 68Ga-labelled tracers in clinical routine? *Eur. J. Nucl. Med. Mol. Imaging* **2007**, *34*, 978–981.
- (25) Henary, M.; Pannu, V.; Owens, E. A.; Aneja, R. Near infrared active heptacyanine dyes with unique cancer-imaging and cytotoxic properties. *Bioorg. Med. Chem. Lett.* **2012**, *22*, 1242–1246.
- (26) Usama, S. M.; Park, G. K.; Nomura, S.; Baek, Y.; Choi, H. S.; Burgess, K. Role of Albumin in Accumulation and Persistence of Tumor-Seeking Cyanine Dyes. *Bioconjugate Chem.* **2020**, *31*, 248–259.
- (27) Acerbi, F.; Broggi, M.; Schebesch, K. M.; Höhne, J.; Cavallo, C.; De Laurentis, C.; Eoli, M.; Anghileri, E.; Servida, M.; Boffano, C.; et al. Fluorescein-Guided Surgery for Resection of High-Grade Gliomas: A Multicentric Prospective Phase II Study (FLUOGLIO). *Clin. Cancer Res.* **2018**, *24*, 52–61.
- (28) Patel, H. P.; Chadwick, D. R.; Harrison, B. J.; Balasubramanian, S. P. Systematic review of intravenous methylene blue in parathyroid surgery. *Br. J. Surg.* **2012**, *99*, 1345–1351.
- (29) Keller, D. S.; Ishizawa, T.; Cohen, R.; Chand, M. Indocyanine green fluorescence imaging in colorectal surgery: overview, applications, and future directions. *Lancet Gastroenterol. Hepatol.* **2017**, *2*, 757–766.
- (30) Schatlo, B.; Fandino, J.; Smoll, N. R.; Wetzel, O.; Remonda, L.; Marbacher, S.; Perrig, W.; Landolt, H.; Fathi, A. R. Outcomes after combined use of intraoperative MRI and 5-aminolevulinic acid in high-grade glioma surgery. *Neuro Oncol.* **2015**, *17*, 1560–1567.
- (31) Manca, G.; Garau, L. M.; Mazzarri, S.; Mazzuca, L.; Muccioli, S.; Ghilli, M.; Naccarato, G.; Colletti, P. M.; Rubello, D.; Roncella, M.; et al. Novel Experience in Hybrid Tracers: Clinical Evaluation of Feasibility and Efficacy in Using ICG-99mTc Nanotop for Sentinel Node Procedure in Breast Cancer Patients. *Clin. Nucl. Med.* **2021**, *46*, e181–e187.
- (32) Doroshow, J. H.; Simon, R. M. On the Design of Combination Cancer Therapy. *Cell* **2017**, *171*, 1476–1478.
- (33) Gai, S.; Yang, G.; Yang, P.; He, F.; Lin, J.; Jin, D.; Xing, B. Recent advances in functional nanomaterials for light-triggered cancer therapy. *Nano Today* **2018**, *19*, 146–187.

(34) Li, T.; Li, C.; Ruan, Z.; Xu, P.; Yang, X.; Yuan, P.; Wang, Q.; Yan, L. Polypeptide-Conjugated Second Near-Infrared Organic Fluorophore for Image-Guided Photothermal Therapy. *ACS Nano* **2019**, *13*, 3691–3702.

(35) Luo, S.; Tan, X.; Qi, Q.; Guo, Q.; Ran, X.; Zhang, L.; Zhang, E.; Liang, Y.; Weng, L.; Zheng, H.; et al. A multifunctional heptamethine near-infrared dye for cancer theranosis. *Biomaterials* **2013**, *34*, 2244–2251.

(36) Modica-Napolitano, J. S.; Aprille, J. R. Delocalized lipophilic cations selectively target the mitochondria of carcinoma cells. *Adv. Drug Delivery Rev.* **2001**, *49*, 63–70.